Helsinki University of Technology Publications in Engineering Physics
Teknillisen korkeakoulun teknillisen fysiikan julkaisuja
Espoo 2008 TKK-F-A853

THERMAL CONDUCTIVITY AND CONTACT RESISTANCE OF COMPRESSED GAS DIFFUSION LAYER OF PEM FUEL CELL

Iwao Nitta, Olli Himanen & Mikko Mikkola

TEKNILLINEN KORKEAKOULU
TEKNISKA HÖGSKOLAN
HELSINKI UNIVERSITY OF TECHNOLOGY
TECHNISCHE UNIVERSITÄT HELSINKI
UNIVERSITE DE TECHNOLOGIE D'HELSINKI

Helsinki University of Technology Publications in Engineering Physics
Teknillisen korkeakoulun teknillisen fysiikan julkaisuja
Espoo 2008 TKK-F-A853

THERMAL CONDUCTIVITY AND CONTACT RESISTANCE OF COMPRESSED GAS DIFFUSION LAYER OF PEM FUEL CELL

Iwao Nitta, Olli Himanen & Mikko Mikkola

Helsinki University of Technology
Faculty of Information and Natural Sciences
Department of Engineering Physics

Distribution:
Helsinki University of Technology
Advanced Energy Systems
P.O. Box 4100
02015 TKK
Finland
URL: http://www.tkk.fi/Units/AES/
Tel. +358-9-451 3198
Fax. +358-9-451 3195

ISBN 978-951-22-9216-5 (PDF)
ISSN 1459-7268 (PDF)
URL: http://lib.tkk.fi/Reports/2008/isbn9789512292165.pdf

Multiprint Oy
Espoo 2008

HELSINKI UNIVERSITY OF TECHNOLOGY
PO Box 1000, FI - 02015 TKK
http://www.tkk.fi/

ABSTRACT

Faculty
Faculty of Information and Natural Sciences

Department
Department of Engineering Physics

Author(s)
Iwao Nitta, Olli Himanen & Mikko Mikkola

Title
Thermal Conductivity and Contact Resistance of Compressed Gas Diffusion Layer of PEM Fuel Cell

Abstract

This paper discusses the effect of compression pressure on the mechanical and thermal properties of gas diffusion layers (GDL). The stress-strain curve of the GDL revealed one nonlinear and two piecewise linear regions within the compression pressure range of 0 to 5.5 MPa. The thermal conductivity of the compressed GDL was found to be independent of the compression pressure and was determined to be 1.18 ± 0.11 W m-1 K-1. The thermal contact resistance between the GDL and graphite was evaluated by augmenting experiments with computer modeling. The thermal contact resistance decreased nonlinearly with increasing compression pressure. According to results here, the thermal bulk resistance of the GDL is comparable to the thermal contact resistance between the GDL and graphite. A simple one dimensional model predicted a temperature drop of 1.7–4.4 ˚C across the GDL and catalyst layer depending on compression pressures.

Keywords (and classification)
Inhomogeneous compression; Gas diffusion layer; PEM Fuel cells; Thermal conductivity; Thermal contact resistance; Stress-strain curve

Place	Month - Year	Language	Number of pages
Espoo, Finland	February 2008	English	15

ISBN (print)	ISBN (electronic)	ISSN (print)	ISSN (electronic)
	978-951-22-9216-5		1459-7268

Serial name
Helsinki University of Technology Publications in Engineering Physics

Serial number or report code
TTK-F-A853

Distribution of the printed publication

Internet access (URL)
http://lib.tkk.fi/Reports/2008/isbn9789512292165.pdf

Table of Contents

1 Introduction

The proton exchange membrane (PEM) fuel cell is under active development because of its relatively low operation temperature, size flexibility, quick start-up, system robustness and pollution free operation. Because of its low operating temperature, typically less than 100 ˚C, the product water often remains in liquid form within the cell. The condensed water may flood the cell which significantly hinders mass transport [1-7]. Therefore, flooding must be properly prevented by e.g. the hydrophobic treatment of components [8]. On the other hand, deficiency of water decreases the proton conductivity of the membrane and thus humidification of reactants is typically needed. Water management has a considerable effect on fuel cell performance and the process is highly sensitive to operational and material parameters [9-13]. Water transport inside the fuel cell has a close link to temperature distribution since water and oxygen diffusivity, saturation parameters, and reaction kinetics are all temperature dependent, see, e.g. [14]. Therefore, extensive modeling studies have been devoted to obtaining an accurate picture of the combined thermal and water transport phenomena, see e.g. [15-17]. Furthermore, accurate prediction of the temperature distribution is of vital importance for achieving better and stable performance of the fuel cell. This is because the temperature distribution caused by inadequate thermal and water management may lead into formation of local hotspots in the cell, which may degrade the cell components and drop the life-time of the cell [18,19].

One of the most common shortcomings of previous studies is disregarding the effect of compression on the physical properties of the cell components. When the fuel cell is assembled, a certain compression pressure must be exerted to achieve adequate contact between the components and to ensure proper gas sealing. This assembling pressure has a significant effect on fuel cell performance [20-23], mainly because of changes in the morphological and physical properties of gas diffusion layers (GDL) and catalyst layers (CL). The GDL and CL in general have highly porous structure because of the requirements set by their functions [24], and the pores of GDL are crushed to some extent when compression pressure is applied. Generally speaking, increasing compression improves the electric conductivity of GDL [25,26] and decreases the contact resistance at the interfaces [27-30]. Furthermore, the preferential pathway for liquid water transport may be created in the compressed part of the GDL [31-33]. While a certain compression pressure is necessary, excessive compression impedes reactant transport by decreasing GDL porosity [34,35] and may also damage typical paper type GDLs and other components [31,36-38]. Thus, an optimum compression pressure and compressed thickness, which trades off these competing issues, has to be identified for each system.

Of particular importance is the fact that the compression pressure over the GDL is inhomogeneous because of the rib/channel structure of the neighboring bipolar plate. In an actual fuel cell assembly, the compression force is exerted practically only on the GDL under the rib of the bipolar plate but not under the channel. As a consequence, thickness of the GDL varies, i.e. the GDL under the rib is deformed and becomes thinner and the GDL under the channel partially intrudes into the channel as seen in Fig. 1.

The thickness variation of the GDL may be a decisive factor for transport phenomena and consequently cell performance. However, only a few modeling studies were found where the thickness variation of the GDL was considered, see e.g. [39-43]. Although those studies provide insight into transport phenomena in the cell, they still leave room for discussion. This is because many parameter values that were used, such as contact resistance or conductivity, are subject to high uncertainty.

Using proper material parameters in models is highly important for studying the local phenomena, which can not be easily interpreted by the polarization curves only. It is often the case that modeled polarization curves obtained from two models which use different assumptions and modeling parameters are quite identical and fit well to the same set of experimental data [44-46]. This is also the case in the authors' previous study, where the polarization curves using previously adopted assumptions agreed fairly well with results from a model which considered the inhomogeneous compression [47]. However, the current density distribution inside the cell was significantly altered when inhomogeneous compression was taken into account, in which the

properties of the GDL were varied according to the thickness. This finding highlights the importance of detailed knowledge of the cell component properties in realistic operating conditions.

So far, information on experimentally evaluated modeling parameters has been limited and further investigation of physical properties of GDLs is essential, especially paying attention to the effect of compression. It should be noted that the effect of compression on the physical properties of the GDL have commonly been investigated as a function of compression pressure. However, correlating this data to conditions inside a fuel cell assembly is not straightforward since the compression pressure exerted onto the GDL depends on the thickness of neighboring gaskets and is different from the cell assembling pressure. In fact, the thickness of the GDL compressed to gasket thickness under the rib as well as its uncompressed thickness under the channel are the only parameters one can set in a realistic fuel cell construction, and they determine the GDL's characteristics. Therefore, the compression effect should be discussed in the light of compressed GDL thickness, not compression pressure. This is also convenient for model construction, since one just needs to change the parameters according to the model geometry when the effect of compression is considered. Therefore, the physical properties of GDL were evaluated as a function of its thickness, and the significant effects of compression have been outlined in ref. [48].

The properties which were not characterized in the authors' previous study are thermal conductivity and thermal contact resistance. To the authors' knowledge, only few experimental assessments of the thermal properties of cell components in sufficient detail have been carried out, e.g. by Khandelwal and Mench [49], and Vie and Kjelstrup [50]. Since it was thought that the thermal properties depended on the compression pressure, further study of compression effect on them was warranted. The purpose of this study, therefore, is to provide comprehensive details on the thermal properties of GDL as a function of its compressed thickness. The results will then be used in a modeling study to achieve deeper understanding of transport phenomena.

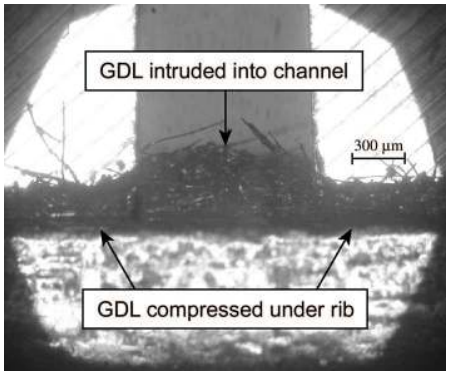

Fig. 1 Cross-sectional view of the GDL and flow field plate taken by optical microscope (OLYMPUS PMG3). The GDL is compressed under the rib and partially intrudes into the channel.

2 Experimental

2.1 Stress-strain behavior of GDL

The stress-strain behavior of the GDL (SGL SIGRACET® 10 BA) was measured with the experimental setup illustrated in Fig. 2. It consists of a base foundation, base plate and support plate fixed to each other with bolts and guiding rods. The dial indicator was installed into an opening in the base plate and base foundation. The GDL sample placed on the base plate was compressed by a steel rod and the weight loaded onto it. The support plate kept the steel rod perpendicular to the GDL sample to ensure even compression onto it. A hole was cut into the center of the circular GDL sample so that the tip of the plunger of the dial indicator had direct contact to the bottom of the steel rod. A clear advantage of this design was the capability to directly measure the deflection of the GDL under compression.

Measurements were conducted using 1 to 4 stacked GDLs. The area of sample GDLs was varied by changing both inner and outer diameter, ranging from 7 to 15 and 12 to 27 mm, respectively, for quantitative analysis. Various compression forces were exerted onto the GDL by increasing the loading weight at 0.5 kg steps up to 82 kg. Although Mathias et al. [24] determined a maximum load of 2.75 MPa for the GDL (Toray TGP-H060), compression pressure up to approximately 5.5 MPa was applied in this study.

It was found that the more GDLs stacked the longer the interval required to achieve the steady state conditions after the weights were loaded. Therefore, the load was increased at 5 to 20 minute intervals, depending on the number of GDL samples under test. Measurements were repeated five times for each sample area and number of stacked GDLs.

The initial deflection of the GDL was found to be fairly susceptible to low compression pressures, probably because of the rough surface of the GDL. Therefore, an additional measurement applying low compression pressures was conducted using a smaller steel rod and lighter weights up to approximately 5 kg (~ 0.1 MPa).

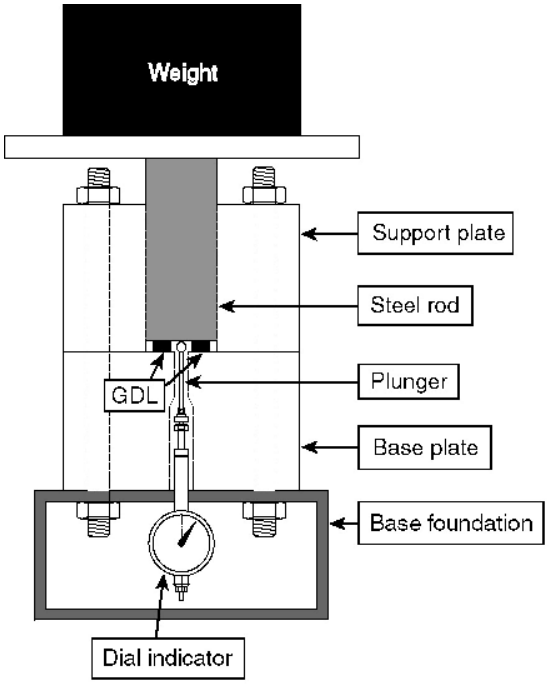

Fig. 2 Schematic of experimental setup for measuring the stress-strain behavior of GDL

2.2 Thermal properties of GDL

2.2.1 Experimental setup and measurements

Fig. 3 shows the experimental setup for measuring the thermal properties of the GDL. Heat flux from the heating element (Watlow Metric FIREROD® Cartridge) embedded in the lower graphite rod transferred from the lower rod to the upper rod through the GDL(s) between them. The graphite rods were constructed so that the end facing to the GDL had a smaller diameter of 20 mm. This shape was found to curb heat transfer through air between the two graphite rods and maximized the heat transfer through the GDL according to an unpublished modeling study by the author.

The graphite rods and GDL samples were thermally insulated from the surroundings by a PVC tube and polystyrene insulator. The temperature of the upper end of the upper graphite rod was maintained at approximately 16 C° by a cooling block (Thermaltake CL-W 0087) through which coolant fluid flowed. A thermostat (Lauda RE 310 chiller with a Lauda E 300 controlled head)

was used to control the coolant temperature and flow. This system allowed constraining the heat dissipation in radial direction and thus, a nearly one-dimensional heat transfer in longitudinal direction was achieved.

GDL samples having an area of 144 mm^2 were placed onto the lower graphite rod. The fixture accommodated 1 to 5 stacked GDL pieces. Measurements were conducted with various compression pressures by changing the weight loaded ranging from 4.7 to 77.8 kg. Corresponding compressed GDLs thicknesses were calculated using the measured stress-strain curve (see Fig. 4).

Temperature probes (Labfacility Pt100/1528 Class A) were located at four points ('A', 'B', 'C' and 'D' in Fig. 3) in the upper and lower graphite rods. Furthermore, an additional temperature probe 'E' was installed in the upper graphite rod in the vicinity of the cooling block to measure the temperature at the graphite rod/cooling block interface. Temperature readings were recorded every 5 seconds with a data logger (Agilent 34970A) until steady-state conditions were achieved. That took typically more than 5 hours.

In order to accurately determine the heat flux transferred through the graphite rods, Q_{GR}, a separate measurement was conducted. The experimental system of this measurement is fundamentally similar to the one shown in Fig. 3, with the exception that the two graphite rods and the GDLs in Fig. 3 were replaced by one long graphite rod, into which temperature probes were embedded. The Q_{GR} was calculated from Fourier's law using the known thermal conductivity of graphite, 128 W m^{-1} K^{-1}, and the temperature drop measured with the temperature probes. For quantitative analysis, two different heating powers were applied, 4.05 and 5.24 W.

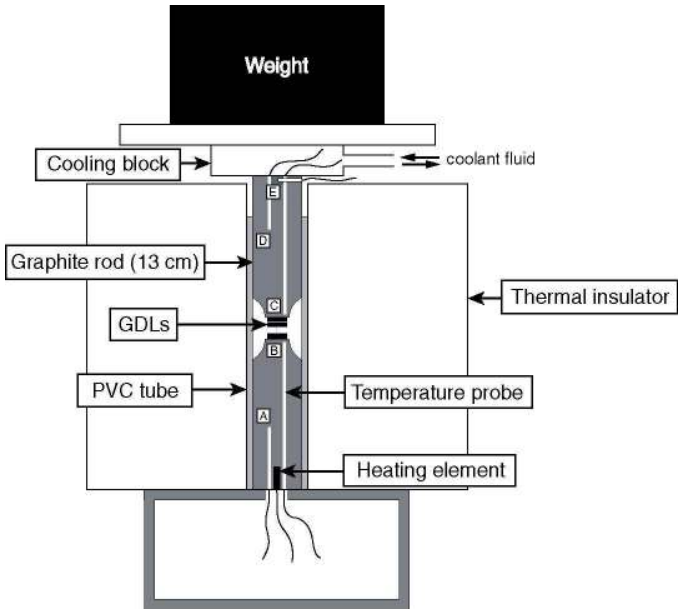

Fig. 3 Schematic of thermal properties measurement system

As discussed previously, changing the compression pressure leads into changes in both electric contact resistance and electric bulk resistance of GDL [48]. This correlation between compression and resistances was expected to hold true also for thermal resistances because of the analogy of electric and heat transfer. Therefore, the authors applied the experimental technique of the previous study to derive the thermal bulk conductivity and thermal contact resistance separately. A brief description of this experiment process is given below, and more details can be found in the previous study [48].

2.2.2 Thermal conductivity of GDL

The measured temperature drop between points 'B' and 'C' (Fig. 3), $\Delta T_{B\text{-}C}$, is a function of the number of GDLs, n, and the compressed GDL thickness, h, and is expressed as

$$\Delta T_{B-C}(h,n) = \left(2R_{c,GDL/GR}(h) + (n-1)\cdot R_{c,GDL/GDL}(h) + n\cdot R_{b,GDL}(h)\right)\cdot Q_{GDL} + 2R_{b,GR}\cdot Q_{GR} \quad (1)$$

where $R_{c,GDL/GR}(h)$ denotes the thermal contact resistance between the GDL and graphite rod, $R_{c,GDL/GDL}(h)$ the thermal contact resistance between two GDLs, $R_{b,GDL}(h)$ the thermal bulk resistance of GDL, $R_{b,GR}$ the thermal bulk resistance of the graphite rod. The heat flux through the GDL, Q_{GDL}, was calculated from GDL sample area and Q_{GR} based on the assumption that heat transfer from graphite and GDL to the air gap was negligibly small.

To eliminate the thermal contact resistance between the GDLs, conductive silver particles were sputtered onto the GDL surfaces. The sputtering process was referred to that in published literature [51,52]. This method has been shown to reduce the contact resistance without affecting the bulk conductivity significantly [53,54]. All GDL surfaces that came into contact with other GDLs were silver coated, but GDL surfaces facing the graphite rods were left untreated to evaluate $R_{c,GDL/GR}(h)$. This procedure allowed eliminating $R_{c,GDL/GDL}(h)$ and reducing Eq. (1) into

$$\Delta T_{B-C}(h,n) = \left(2R_{c,GDL/GR}(h) + n\cdot R_{b,GDL}(h)\right)\cdot Q_{GDL} + 2R_{b,GR}\cdot Q_{GR} \quad (2)$$

Thus, plotting $\Delta T_{B\text{-}C}$ as a function of the number of GDLs, the slope of the graph, S, gives the value of $R_{b,GDL}(h)\cdot Q_{GDL}$.

The thermal bulk conductivity of the GDL, $\kappa_{GDL}(h)$, can be expressed with $R_{b,GDL}(h)$ and the compressed GDL thickness h as:

$$\kappa_{GDL}(h) = \frac{h}{R_{b,GDL}(h)} = \frac{h}{S}Q_{GDL} \quad (3)$$

For the calculation of the $\kappa_{GDL}(h)$, the evaluated h (see Fig. 4) were used based on the assumption that the values of h depend on the compression pressure but not on the number of stacked GDLs.

2.2.3 Thermal contact resistance between GDL and graphite

For determining the thermal contact resistance between the GDL and graphite rod, $R_{c,GDL/GR}(h)$, a 3D model corresponding to the experimental apparatus (Fig. 3) was constructed using a commercial finite element method solver software (COMSOL Multiphysics 3.2a). This procedure was adopted because it was believed to be difficult to separate the contact resistance from the total resistance experimentally.

The temperature distribution in the system was solved using the measured values for thermal conductivities and calculated heat flux and varying the GDL thickness from 129 to 328 μm corresponding to the experimental work. The unknown parameter, $R_{c,GDL/GR}(h)$, was varied until the resulting temperature profile corresponded to the measured values.

The temperature profiles in the graphite rod, T_{GR}, and the GDL, T_{GDL}, were modeled using the governing equation for heat flux which follows from the Fourier's law:

$$\nabla^2 T = \nabla\cdot\left(-\kappa_{GR}\nabla T_{GR}\right) = \nabla\cdot\left(-\kappa_{GDL}\nabla T_{GDL}\right) = 0 \quad (4)$$

It should be noted that the thermal conductivity of the GDL was assumed to be isotropic, i.e. same value in both in- and through-plane directions. Because of $R_{c,GDL/GR}(h)$, the temperature profile becomes discontinuous. At the GDL/graphite rod interface, a Neumann boundary condition was applied,

$$-\bar{n}\cdot\left(-\kappa_{GR}\nabla T_{GR}\right) = \frac{T_{GR} - T_{GDL}}{R_{c,GDL/GR}(h)} \quad (5)$$

where $\overline{n}$ is the surface normal vector.

At the boundary between the upper graphite rod and cooling block, a constant temperature boundary condition was applied, using the temperatures measured by the temperature probe, 'E' (see Fig. 3). At the graphite rod/PVC tube interface, graphite rod/air interface and GDL/air interface, Neumann boundary conditions were applied for the thermal flux. The thermal contact resistances at the rod/PVC tube interface and heat transfer coefficient at the graphite rod/air and the GDL/air interfaces were based on estimations. They were varied within reasonable limits and ascertained not to affect the temperature distribution significantly. The thermal contact resistance between the PVC and insulator was not included in the model due to negligible effect on the temperature distribution inside the graphite rods.

At the boundary between heating element and graphite rod, a boundary condition for the heat flux from the heating element, Q_{HE}, was applied,

$$-\overline{n}\cdot\left(-\kappa_{GR}\nabla T_{GR}\right)=Q_{HE} \tag{6}$$

The value of Q_{HE} was set so that the temperature profile in a separate model in which one long graphite rod was used matched the experimental results. The same value of Q_{HE} was applied to the model with two graphite rods and GDL, based on the assumption that heat loss in the radial direction was the same in both cases.

3 Results and Discussion

3.1 Stress-strain behavior of the GDL

The thickness of uncompressed GDL, which was 380 µm reported by the manufacturer, was determined to be 370 ± 10 µm in a separate measurement with a low compression pressure. This thickness was set as a base point and the stress-strain curve was calculated from the measured thickness-pressure pairs. Fig. 4 shows the stress-strain curves of a GDL, calculated from measurement results with 1 to 4 GDLs. The results from the two separate measurements using low (up to 0.1 MPa) and high compression pressure (0.1 to 5.5 MPa) were ascertained to coincide well. The area of the GDL sample was found not to affect the stress-stain curve as long as the compression pressure was the same.

The most noticeable variations in GDL strain were found with the low compression pressure (~ 0.2 MPa), as reported in literature, see, e.g. [24,27,35,38]. This is most probably due to the smoothening of the rough surface of the GDL. At a compression pressure above 1 MPa, two piecewise linear regions were identified in the range from 1 to 3.5 MPa, and from 3.5 to 5.5 MPa as also seen in ref. [27]. This was probably because of the nature of the GDL. Typical paper type GDLs have two different pore diameter regions, namely, hydrophobic pores and hydrophilic pores, see e.g. [23,55-57]. The first linear region may be associated to the crushing of hydrophilic pores, and the second to the crushing of hydrophobic pores.

Although the curves obtained with different number of GDLs indicated almost identical compressive behavior, the strain of each GDL decreased as more GDLs were stacked. This was most probably due to the fact that stress-strain behavior of the interface of two rough GDL surfaces is different from that of the GDL/graphite interface or bulk GDL. However, the properties of the bulk GDL or interface between the GDL and graphite do not depend on the number of the stacked GDLs. For the purposes of evaluating the thermal properties, when more than one GDLs were used each GDL was assumed to follow the same stress-strain curve.

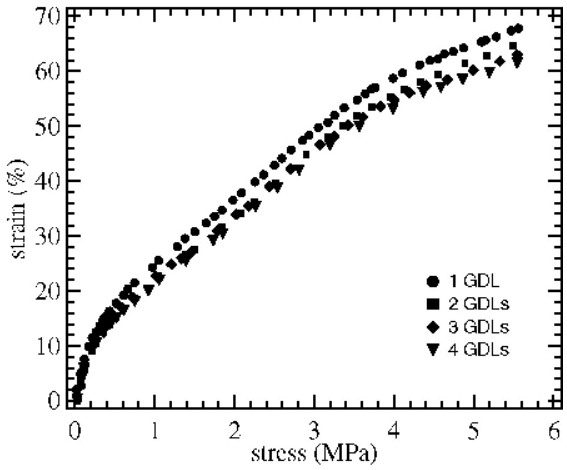

Fig. 4 Stress-strain curve of the GDL measured with different number of GDLs

3.2 Thermal conductivity of GDL

The measured temperature drops between the points 'B' and 'C', $\Delta T_{B\text{-}C}$, as a function of the number of GDLs are shown in Fig. 5. Fig. 5 includes the $\Delta T_{B\text{-}C}$ when GDL(s) were compressed to various thicknesses, from 328 to 129 µm. When a higher compression pressure was applied and GDL thickness decreased, a lower $\Delta T_{B\text{-}C}$ was observed. This was because both thermal bulk and contact resistances of the GDL decreased with compression pressure.

The $\Delta T_{B\text{-}C}$ increased linearly with the number of GDLs. Since thermal contact resistances between GDLs, $R_{c,GDL/GDL}(h)$, were eliminated by sputtering, the slopes of the $\Delta T_{B\text{-}C}$ as a function of the number of GDLs reflected the thermal bulk resistance of the GDL as described in Section 2.2.2.

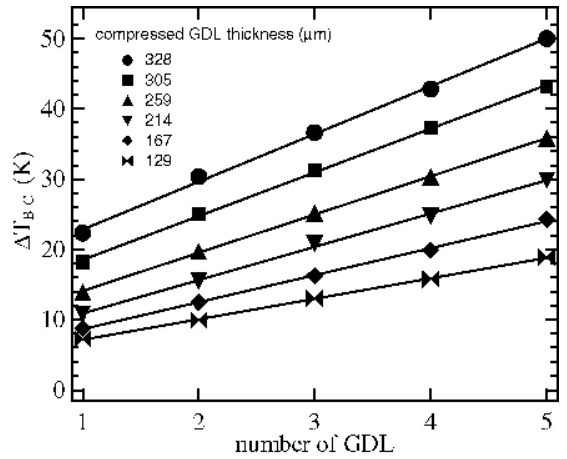

Fig. 5 Temperature drops between the points 'B' and 'C' as a function of number of stacked GDL

The heat fluxes through the graphite, Q_{GR}, were determined to be 3.33 and 4.45 kW m^{-2} at heating powers of 4.05 and 5.24 W, respectively. The resulting thermal conductivity of the GDL, $\kappa_{GDL}(h)$, as a function compressed GDL thickness is shown in Fig. 6. The error bars shown in the Fig. 6 were estimated considering the following error sources; 1) errors of the measured temperature inside the graphite rods, i.e. the gradient of the $\Delta T_{B\text{-}C}$ in Fig. 5, 2) heat leakage in the radial direction from the system, i.e. change in heat flux passing through the graphite rods and the GDLs, 3) variation in thickness of initial and compressed GDL, and 4) fluctuation in set temperature at the end of upper graphite rod. This analysis was conducted with the method adopted in a previous study [49]. The margins of error shown in the figure represent the 90% confidence interval.

An important finding is that the $\kappa_{GDL}(h)$ does not depend on compression and was determined to be 1.18 ± 0.11 W m^{-1} K^{-1}. It was expected that higher compression pressure would reduce $\kappa_{GDL}(h)$ as observed for electric conductivity [48], since carbon fibers in the GDL have better contact to each other under compression, and the volume of poorly conducting air in the pores is reduced. However, this was not the case and the interrelation between compression and heat transport through the GDL was found to be different from that between compression and electric transport.

The $\kappa_{GDL}(h)$ obtained here is approximately four times higher than the reported value (0.3 W m^{-1} K^{-1} at approximately 2 MPa) [23,49,50]. This difference is probably due to the fact that in the previous study, the contribution of $R_{c,GDL/GDL}(h)$ was simply neglected in calculation of $\kappa_{GDL}(h)$ [49] or $R_{b,GDL}(h)$ was not properly derived from the measured temperature gap [23]. If the $R_{c,GDL/GDL}(h)$ is not eliminated by e.g. the process implemented in this study, the resulting $R_{b,GDL}(h)$ will contain also the contact resistances, and thus underestimate the $\kappa_{GDL}(h)$.

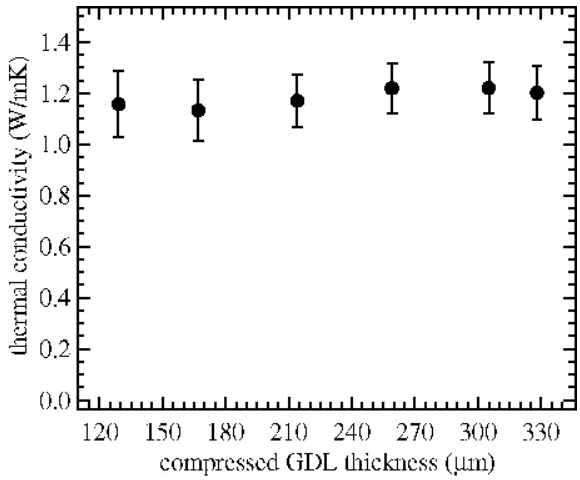

Fig. 6 Thermal conductivity of GDL as a function of compressed GDL thickness

3.3 Thermal contact resistance between GDL and graphite

The area-specific thermal contact resistance between the GDL and graphite rod, $R_{c,GDL/GR}(h)$, is shown in Fig. 7. The $R_{c,GDL/GR}(h)$ decreased nonlinearly as the GDL was compressed. Higher compression increased the actual contact area at the interface between the GDL and graphite, thus decreasing contact resistance. Error estimates were obtained by repeating the simulation with varying the modeling parameters; 1) the thermal bulk resistance of GDL, 2) the heat fluxes, and 3) the measured temperatures.

The $R_{c,GDL/GR}(h)$ at an approximate compression pressure of 2.2 MPa (compressed GDL thickness of ca. 233 μm), $0.65 \pm 0.18 \times 10^{-4}$ m^2 K W^{-1}, is smaller than the value reported in the literature [49], 1.5×10^{-4} m^2 K W^{-1}. A possible reason for this is that the material in contact with the GDL is different. Khandelwal and Mench used aluminum bronze [49], while graphite was used in this study.

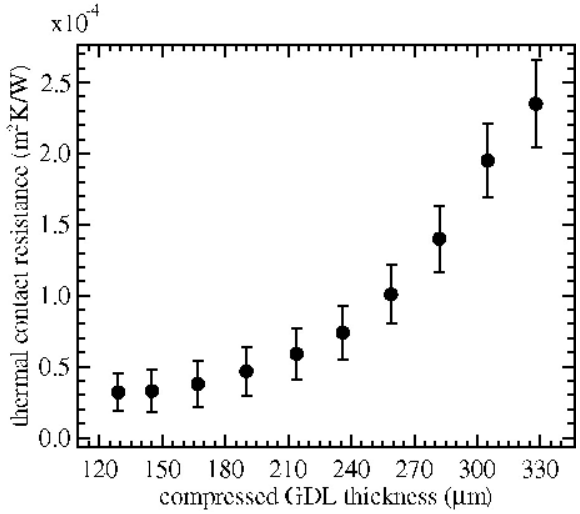

Fig. 7 Thermal contact resistance between GDL and graphite as a function of compressed GDL thickness

The temperature profiles of the system with various compressed GDL thicknesses obtained from the simulations are plotted in Fig. 8(a), which includes also the measured temperatures at points 'A', 'B', 'C' and 'D' in the graphite rods (see Fig. 3). To clarify the contribution from $R_{c,GDL/GR}(h)$ and $R_{b,GDL}(h)$ to temperature drop, the temperature profile in the vicinity of the GDL interfaces is enlarged in Fig. 8(b). It has been often speculated that the interface is a larger source of thermal resistance than the bulk GDL. However, the $R_{b,GDL}(h)$ accounts for more than 30% of the total thermal resistance of the GDL at low compression and for more than 50% of the total thermal resistance when the GDL was compressed to less than 70% of initial thickness (below 259 μm).

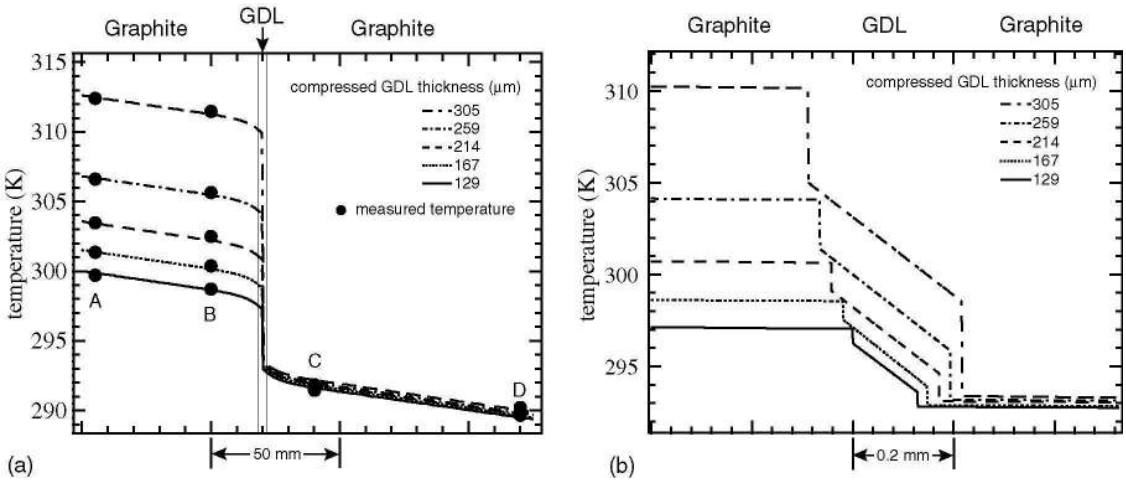

Fig. 8 Modeled temperature profile and measured temperature (a) region around temperature measured point, and (b) enlarged in the vicinity of GDL

4 Modeled temperature drop in a fuel cell

Temperature profile inside a fuel cell was calculated using a simple one dimensional model. This model is a modified version of the one by Khandelwal et al. [49].

The governing equation of heat transfer is expressed with the thermal conductivity of component i, κ_i, and temperature, T, as

$$\nabla \cdot (\kappa_i \nabla T) = S_e \tag{7}$$

where S_e, is the heat source, written as

$$S_e = \frac{j^2}{\sigma_i} + \frac{j}{h_{CL}}\left(\frac{T\Delta S}{zF} + \eta\right) \tag{8}$$

where j denotes the current density, σ_i the electric conductivity of component i, h_{CL} the thickness of catalyst layer, ΔS the change in entropy, z the number of electrons participating in the reaction, F the faraday constant, η the overpotential including activation, concentration and ohmic losses. In the electrolyte membrane and GDL, S_e includes only the Joule heating, the first term of right member in Eq. (8). In the catalyst layer, the second and third terms are also included, representing entropic heat of reaction and irreversible heat of electrochemical reaction, respectively.

The thickness of GDL was changed from 129 to 328 μm in the model, where the κ_{GDL} was constant and assumed to be isotopic. The boundary between the GDL and graphite was converted to a pseudo-thin layer having thickness of 10 μm. The thermal conductivity of this layer was calculated from the $R_{c,GDL/GR}(h)$. The electric contact resistance between GDL and graphite evaluated in authors' previous study [48] was also converted to the electric conductivity of this thin layer. However, heat production from the electric contact resistance was ascertained to be small enough not to affect the temperature profile. Instead of the thermal contact resistance between the GDL and CL and thermal bulk resistance of CL, the effective thermal resistance of the CL evaluated by Khandelwal et al. [49] was used. Temperature was set constant at outer ends of graphite bipolar plates. Symmetry boundary conditions were applied to all boundaries except those associated with heat generation. All the model parameters are listed in Table 1.

Table 1 Cell design parameters and material properties

Parameter	Value
GDL thickness	129–328 μm
CL thickness	25 μm
Membrane thickness	50 μm
Graphite plate thickness	1 mm
Effective thermal conductivity of CL	0.27 W m^{-1} K^{-1} [49]
Effective electric conductivity of CL	320 S m^{-1} [48]
Electric conductivity of GDL	2203–535 S/m [48]
Thermal conductivity of GDL	1.18 W m^{-1} K^{-1}
Ionic conductivity of membrane and CL	5.09 S m^{-1} [58]
Thermal conductivity of membrane	0.12 W m^{-1} K^{-1} [49]
Thermal conductivity of graphite bipolar plate	128 W m^{-1} K^{-1}
Thermal contact resistance between GDL and graphite	3.2×10^{-5}–2.35×10^{-4} m^2 K W^{-1}
Temperature at outer edge of graphite bipolar plates	80 ˚C
Current density	1.0 A cm^{-2}
Anode overpotential	0.01 V
Cathode overpotential	-0.75 V
Entropy change of anode reaction [-1]	0.104 J mol^{-1} K^{-1}
Entropy change of cathode reaction[1]	-326.36 J mol^{-1} K^{-1}

The resulting temperature profile across the cell components was identical to the one shown in [49]. The temperature drop from the highest temperature point, i.e. the interface between the membrane and cathode CL to the lowest temperature point, i.e. the outer edge of the graphite plate as a function of compressed GDL thickness is shown in Fig. 9. The temperature drop decreased as the GDL was compressed due to decrease of both thermal bulk and contact resistances. Although the values of temperature drop predicted here were smaller than those reported in the literature, see, e.g. [16,49], the change in temperature drop because of compression should be worth considering in the future.

One missing parameter in this model is the electric contact resistance between the GDL and CL. This contact resistance is comparable to the membrane resistance [59] and can be one of the major heat sources. A detailed modeling study considering the compression effect and taking into account all these important parameters is under way by the author.

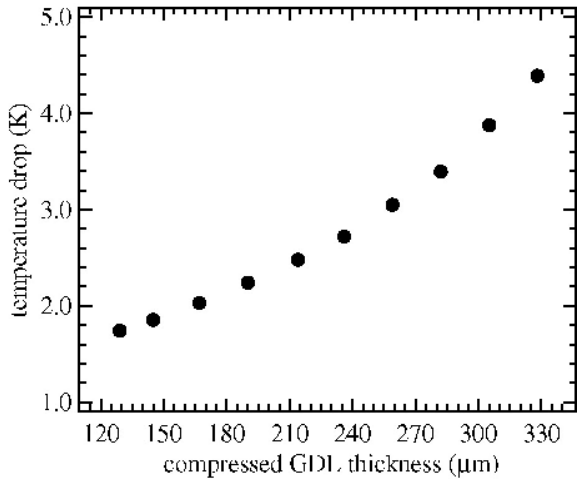

Fig. 9 Calculated temperature drop inside the cell as a function of compressed GDL thickness

5 Summary and conclusions

The purpose of this study was to evaluate the mechanical and thermal properties of the GDL experimentally as a function of compression. The stress-strain curve of the GDL revealed one nonlinear and two linear regions as the compression pressure was increased up to 5.5 MPa. This was probably because of the nature of the GDL, i.e. a rough surface and void volume consisting of pores with two different pore diameter ranges. The thermal conductivity of GDL was found not to depend on compression pressure. The obtained value of the thermal conductivity of GDL, 1.18 ± 0.11 W m^{-1} K^{-1}, was approximately four times larger than those reported in the literature.

The thermal contact resistance between GDL and graphite decreased nonlinearly with increasing compression pressure. This may be attributed to the increase in actual contact area at the interface as compression pressure was increased. The thermal bulk resistance of the GDL was comparable to the thermal contact resistance between the GDL and graphite, suggesting both bulk and interface of the GDL should be considered properly in modeling studies.

A simple one-dimensional model of a fuel cell employing the evaluated thermal parameters showed that the temperature drop inside the fuel cell decreased as the GDL was compressed more. The predicted temperature drop across the GDL and CL ranged from 1.7 to 4.4 ˚C for the compressed GDL thickness from 129 to 328 μm correspondingly. Uneven temperature distribution may cause local overheating and lead into the degradation of the cell components and

thus, fuel cell has to be carefully designed to minimize the harmful effects of inhomogeneous compression.

Acknowledgements

The financial support of Fortum Foundation is gratefully acknowledged. In addition, authors wish to thank Dr. Masashi Nakamoto from the laboratory of Metallurgy at the Helsinki University of Technology for instruction in optical microscopy and Dr. Sergey Novikov from Electron Physics laboratory at the Helsinki University of Technology for silver coatings.

References

1 G. Lin, W. He, T.V. Nguyen, J. Electrochem. Soc. 151 (2004) A1999–A2006.

2 G. Lin, T.V. Nguyen, J. Electrochem. Soc. 152 (2005) A1942–A1948.

3 D. Natarajan, T.V. Nguyen, J. Electrochem. Soc. 148 (2001) A1324–A1335.

4 D. Natarajan, T.V. Nguyen, J. Power Sources 115 (2003) 66–80.

5 N.P. Siegel, M.W. Ellis, D.J. Nelson, M.R. Spakovsky, J. Power Sources 128 (2004) 173–184.

6 Z. Liu, Z. Mao, C. Wang, J. Power Sources 158 (2006) 1229–1239.

7 Z.H. Wang, C.Y. Wang, K.S. Chen, J. Power Sources 94 (2001) 40–50.

8 D. Bevers, R. Rogers, M.V. Bradke, J. Power Sources 63 (1996) 193–201.

9 J.H. Nam, M. Kaviany, Int. J. Heat Mass Transfer 46 (2003) 4595–4611.

10 K. Wiezel, P. Gode, G. Lindbergh, J. Electrochem. Soc. 153 (2006) A759–A764.

11 M. Grujicic, K.M. Chittajallu, Chem. Eng. Sci. 59 (2004) 5883–5895.

12 F. Y. Zhang, X. G. Yang, and C. Y. Wang, J. Electrochem. Soc. 153 (2006) A225–A232.

13 U. Pasaogullari, C.Y. Wang, J. Electrochem. Soc. 151 (2004) A399–A406.

14 M. Coppo, N.P. Siegel, M.R. Spakovsky, J. Power Sources 159 (2006) 560–569.

15 K.Z Yao, K. Kran, K.B. McAuley, P. Oosthuizen, B. Peppley, T. Xie, Fuel Cell 4 (1) (2004) 3–29.

16 M. Noponen, E. Birgersson, J. Ihonen, M. Vynnycky, A. Lundblad, G. Lindbergh, Fuel Cells 4 (4) (2004) 365–377.

17 H. Ju, C.Y. Wang, S. Cleghorn, U. Beuscher, J. Electrochem. Soc. 152 (2005) A1645–A1653.

18 J. Ihonen, Ph.D thesis 2003, KTH, Sweden.

19 M Cai, M.S. Ruthkosky, B. Merzougui, S. Swathirajan, M.P. Balogh, S.H. Oh, J. Power Sources 160 (2006) 977–986.

20 W.K. Lee, C.H. Ho, J.W.V. Zee, M. Murthy, J. Power Sources 84 (1999) 45–51.

21 J. Ge, A. Higier, H. Liu, J. Power Sources 159 (2006) 922–927.

22 S.J. Lee, C.D. Hsu, C.H. Huang, J. Power Sources 145 (2005) 353–361.

23 J. Ihonen, M. Mikkola, G. Lindbergh, J. Electrochem. Soc. 151 (8) 2004 A1152–A1161.

24 M. Mathias, J. Roth, J. Fleming, W. Lehnert, Handbook of Fuel Cells Fundamentals, Technology and Applications, Volume 3 Chap. 46 2003, John Wiley & Sons, Ltd.

25 T. Tomimura, S. Nakamura, H. Nonami, H. Saito, 2001 IEEE 7th International Conference on Solid Dielectrics, (2001) 101–104.

26 N. Cunningham, M. Lefévre, G. Lebrun, J.P. Dodelet, J. Power Sources 143 (2005) 93–102.

27 V. Mishra, F. Yang, R. Pitchumani, J. Fuel Cell Sci. Technol. 1 (2004) 2–9.

28 H. Wang, J.A. Turner, J. Power Sources 128 (2004) 193–200.

29 J. Ihonen, F. Jaouen, G. Lindbergh, G. Sundholm, Electrochim. Acta 46 (2001) 2899–2911.

30 P. M. Wilde, M. Mandle, M. Murata, N. Berg, Fuel Cells 4 (3) (2004) 180–184.

31 A. Bazylak, D. Sinton, Z.S. Liu, N. Djilali, J. Power Sources 163 (2007) 784–792.

32 C. Lim, C.Y. Wang, J. Power Sources 113 (2003) 145–150.

33 E.C. Kumbur, K.V. Sharp, M.M. Mench, J. Electrochem. Soc., 154 (12) (2007) B1305–B1314

34 H. Dohle, R. Jung, N. Kimiaie, J. Mergel, M. Müller, J. Power Sources 124 (2003) 371–384.

35 C. Lee, W. Mérida, J. Power Sources 164 (2007) 141–153.

36 T. Matsuura, M. Kato, M. Hori, J. Power Sources 161 (2006) 74–78.

37 C. Xu, T.S. Zhao, Q. Ye, Electrochim. Acta 51 (2006) 5524–5531.

38 S. Escribano, J.F. Blachot, J. Etheve, A. Morin, R. Mosdale, J. Power Sources 156 (2006) 8–13.

39 P. Zhou, C.W. Wu, G.J. Ma, J. Power Sources 163 (2007) 874–881.

40 P. Zhou, C.W. Wu, G.J. Ma, J. Power Sources 159 (2006) 1115–1122.

41 P. Zhou, C.W. Wu, J. Power Sources 170 (2007) 93–100.

42 W. Sun, B.A. Peppley, K. Karan, J. Power Sources 144 (2005) 42–53.

43 V.P. Schulz, J. Becker, A. Wiegmann, P.P. Mukherjee, C.Y Wang, J. Electrochem. Soc. 154 (2007) B419–B426.

44 W.Q. Tao, C.H. Min, X.L. Liu, Y.L. He, B.H. Yin, W. Jiang, J. Power Sources 160 (2006) 359–373.

45 C.H. Min, Y.L. He, X.L. Liu, B.H. Yin, W. Jiang, W.Q. Tao, J. Power Sources 160 (2006) 374–385.

46 H. Ju, C.Y.Wang, J. Electrochem. Soc. 151 (2004) A1954–A1960.

47 T. Hottinen, O. Himanen, S. Karvonen, I. Nitta, J. Power Sources 171 (2007) 113–121.

48 I. Nitta, T. Hottinen, O. Himanen and M. Mikkola, J. Power Sources 171 (2007) 26–36.

49 M. Khandelwal, M.M. Mench, J. Power Sources 161 (2006) 1106–1115.

50 P.J.S. Vie, S. Kjelstrup, Electrochim. Acta 49 (2004) 1069–1077.

51 A. Caillarda, P. Braulta, J. Mathiasa, C. Charlesb, R.W. Boswellb, T. Sauvage, Surf. Coatings Technol. 200 (2005) 391–394.

52 K.L. Huang, Y.C Lai, C.H Tsai, J. Power Sources 156 (2006) 224–231.

53 M. Yamaguchi, N. Matsuo, S. Uozumi, Japanese Patent H6-84529 (1994) (in Japanese).

54 K. Kodama, Japanese Patent P2004-178893A (2004) (in Japanese).

55 J.T. Gostick, M.W. Fowler, M.A. Ioannidis, M.D. Pritzker, Y.M. Volfkovich, A. Sakars, J. Power Sources 156 (2006) 375–387.

56 A. Jena, K. Gupta, Characterization of Pore Structure of Fuel Cell Components Containing Hydrophobic and Hydrophilic Pores, 41st Power Sources Conference, 2005.

57 J. Benziger, J. Nehlsen, D. Blackwell, T. Brennan, J. Itescu, J. Membr. Sci. 261 (2005) 98–106.

58 S. Cleghorn, J. Kolde and W. Liu, Handbook of Fuel Cells – Fundamentals, Technology and Applications, Edited by Wolf Vielstich, Hubert A. Gasteiger, Arnold Lamm. Volume 3: Fuel Cell Technology and Applications. 2003 John Wiley & Sons, Ltd.

59 I. Nitta, O. Himanen, M. Mikkola, Electrochem. Commun. 10 (2008) 47–51.

ISBN 978-951-22-9216-5 (PDF)
ISSN 1459-7268 (PDF)